

# Potential-Dependent Sum Frequency Generation Study of 5-Methylbenzotriazole on Polycrystalline Copper, Platinum, and Gold

Casey Romero and Steven Baldelli\*

Department of Chemistry, University of Houston, Houston, Texas 77204

Received: February 25, 2006; In Final Form: May 2, 2006

In situ sum frequency generation vibrational spectroscopy, at varied potentials and polarization combinations, was performed on polycrystalline copper, polycrystalline platinum, and polycrystalline gold samples in 0.5 M HClO<sub>4</sub> with 50 mM 5-methylbenzotriazole (5-methylBTAH) added. These studies were performed to determine the orientation of 5-methylBTAH on the surface at different potentials. For copper surfaces, orientation of the molecule on the surface is not affected by potential within the potential window studied (−500 to −100 mV vs saturated calomel electrode (SCE)). Sum frequency generation spectra of 5-methylBTAH on platinum show a change in orientation over the potential range studied (−250 to 750 mV vs SCE). The orientation of the methyl group tilts more toward the plane of the interface as the potential is scanned in the positive direction. This orientation change is correlated to hydrogen coadsorption on the platinum surface at low potentials. 5-Methylbenzotriazole lies in the surface plane or does not orient on gold at lower potentials but the orientation is tilted toward normal at more positive potentials over the potential range studied (−500 to 900 mV vs SCE). To compliment these results, cyclic voltammetry and electrochemical impedance spectroscopy measurements were performed. Cyclic voltammograms of copper show that addition of 5-methylBTAH protects the surface from copper dissolution, increasing the electrochemical window by 450 mV. Cyclic voltammetry of 5-methylBTAH on platinum showed a partial blockage of adsorbed hydrogen and also prevented the adsorption of oxygenated species at 450–600 mV. Cyclic voltammetry on gold shows that 5-methylBTAH blocks oxide formation for 400 mV thus increasing the electrochemical window. Electrochemical impedance spectroscopy has been performed to determine the potential of zero charge of 5-methylBTAH on copper.

## Introduction

Benzotriazole (C<sub>6</sub>H<sub>4</sub>N<sub>3</sub>H, BTAH) has been widely used as a corrosion inhibitor for copper and its alloys.<sup>1</sup> The chemisorption of BTAH on copper has been investigated by electrochemical methods,<sup>2–4</sup> scanning probe techniques,<sup>2,3,5</sup> and spectroscopic measurements.<sup>4,6–12</sup> These studies show that BTAH forms an adsorbed adlayer at negative potentials and acidic pH, whereas the loss of the amine hydrogen at more positive potentials and basic pH causes a polymerized Cu(I)–BTAH complex to form.<sup>13</sup> Scanning tunneling microscopy images show that a benzotriazole adlayer is dependent on the anions present as well as the crystal structure of the substrate.<sup>2</sup> It has been shown that substitution of a methyl group on the triazole ring (positions 1–3 in Figure 1) decreases the inhibiting efficiency dramatically whereas alkyl substitution on the benzene ring (positions 4–7 in Figure 1) produces the opposite effect.<sup>9</sup> This is attributed to the hydrophobic character of the methyl group. A higher inhibition efficiency for 5-methylbenzotriazole (5-methylBTAH, Figure 1) than for benzotriazole has been reported.<sup>9</sup> To develop a better understanding of the mechanism for adsorption of benzotriazole on a copper surface, potential-dependent sum frequency generation (SFG) spectroscopy was used to study 5-methylBTAH. 5-Methylbenzotriazole has been chosen for this study because of its higher inhibition efficiency and the methyl group will allow for the probing of the C–H stretching region (2800–3100 cm<sup>−1</sup>). Because 5-methylBTAH is a planar mol-

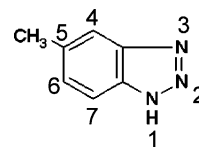


Figure 1. 5-Methylbenzotriazole.

ecule, determination of the orientation of the methyl group should predict the orientation of the entire molecule. Only one other study of benzotriazole in situ using SFG has been reported.<sup>10</sup> That study focused on the ring stretching region (1350–1600 cm<sup>−1</sup>), whereas this study will be probing the C–H stretching region. An understanding of the interfacial structure and its potential dependence is necessary to describe corrosion inhibition at an interface.

The molecular nonspecificity of electrochemical techniques requires the use of surface-sensitive spectroscopic techniques to probe the structure and chemical composition of the electrochemical interface in situ. Linear optical techniques are hampered by the large contribution from the bulk, leading to difficulty in extracting the necessary contribution from the interface. Second-order nonlinear optical processes are only sensitive to noncentrosymmetric environments and are therefore highly surface-sensitive. Sum frequency generation vibrational spectroscopy has the ability to probe buried interfaces in situ.<sup>14</sup> Sum frequency generation is only sensitive to molecules at interfaces where the centrosymmetry of isotropic bulk phases is broken.<sup>15–17</sup> By analysis of the different polarization combinations the orientation of molecules adsorbed at surfaces can

\* Author to whom correspondence should be addressed. E-mail: SBaldelli@uh.edu.

be estimated. The goal of this paper is to compare the effect of potential on an adsorbed adlayer of 5-methylBTAH oriented on the surface of polycrystalline copper, platinum, and gold. 5-Methylbenzotriazole was adsorbed to platinum and gold electrodes to better understand how it adsorbs to noble metal surfaces to compare its adsorption to a copper electrode.

### Sum Frequency Generation

Sum frequency generation spectroscopy is a nonlinear technique used to investigate vibrational resonances of molecules at an interface. With SFG, a tunable infrared laser beam and a fixed frequency visible laser beam are overlapped at the surface both spatially and temporally, and the emitted light at the sum of the frequency of the two input fields is detected ( $\omega_1 + \omega_2 = \omega_s$ ). As the infrared frequency is scanned, increases in amplitude are due to vibrational resonances of molecules at the interface. More specifically, the intensity of the sum frequency beam depends on the intensities of the incident beams,  $E_{\text{vis}}$  and  $E_{\text{IR}}$ , and the second-order nonlinear susceptibility,  $\chi^{(2)}$

$$I(\omega_{\text{sum}}) \approx |K_{\text{sf}}\chi^{(2)}K_{\text{vis}}E_{\text{vis}}K_{\text{IR}}E_{\text{IR}}|^2 \quad (1)$$

$K_{\text{sf}}$ ,  $K_{\text{vis}}$ , and  $K_{\text{IR}}$  are the Fresnel factors of the emitted sum frequency, incident visible, and infrared beams, respectively. The Fresnel factors relate the incident electric fields with the local fields at the surface. They are a function of the angles of incidence and emission at the three wavelengths and on the refractive index of each medium, respectively.

$\chi^{(2)}$  is a third-rank tensor of second order and therefore vanishes with inversion symmetry. Within the electric dipole approximation, no signal arises from molecules in solution and is due only to molecules at an interface where the isotropic environment of the bulk phase is broken.  $\chi^{(2)}$  contains a sum of resonant  $\chi_{\text{R}}^{(2)}$  and nonresonant contributions  $\chi_{\text{NR}}^{(2)}$ . The resonant portion is from vibrational modes of adsorbed molecules on the surface, and the nonresonant contributions are primarily due to the nonlinear response of the metal substrate

$$\chi^{(2)} = \chi_{\text{NR}}^{(2)} + \sum \chi_{\text{R}}^{(2)} \quad (2)$$

Interpretation of sum frequency vibrational spectra is complicated because  $\chi^{(2)}$  contains contributions from several vibrational modes and the nonresonant background of the substrate. Sum frequency generation spectra are fit with the following equation, which assumes that the vibrational resonances follow a Lorentzian line shape

$$I_{\text{SFG}} \propto |\chi_{\text{NR}}^{(2)} + \chi_{\text{R}}^{(2)}|^2 = \left| \chi_{\text{NR}}^{(2)} + \sum_q \frac{A_q}{\omega_{\text{IR}} - \omega_q + i\Gamma_q} \right|^2 \quad (3)$$

where  $q$  is the  $q$ th resonant vibrational mode of the adsorbates.  $A_q$ ,  $\omega_{\text{IR}}$ ,  $\omega_q$ , and  $\Gamma_q$  are the amplitude, scanning IR frequency, the  $q$ th resonant vibrational frequency of the adsorbate, and the line width, respectively.

The intensity of the sum frequency signal is dependent on  $|\chi^{(2)}|^2$ , and therefore the resonant and nonresonant contributions are convoluted. Interference between these contributions gives rise to several different line shapes. The two contributions can add constructively to give a peak, destructively to give a dip, or a combination of the two to give a derivative line shape, depending on the relative phases and strengths of  $\chi_{\text{R}}^{(2)}$  and  $\chi_{\text{NR}}^{(2)}$ .

The resonant portion of  $\chi^{(2)}$ , which is a macroscopic property of the interface, can be related to the hyperpolarizability of the individual molecules in the monolayer,  $\beta$ , by

$$\chi_{\text{R}}^{(2)} = N\langle\beta\rangle \quad (4)$$

$N$  is the number of molecules contributing to the signal per unit area, and  $\langle\beta\rangle$  is the molecular hyperpolarizability orientationally averaged. The hyperpolarizability is a product of the Raman polarizability,  $\alpha$ , and the transition dipole moment of the molecule,  $\mu$ , and therefore all resonances in SFG spectroscopy must be both infrared- and Raman-active

$$\beta_{abc} = \langle g|\alpha_{ab}|v\rangle\langle v|\mu_c|g\rangle \quad (5)$$

The lowercase letters ( $abc$ ) refer to the molecular coordinates that must be transformed to a laboratory fixed coordinate system ( $xyz$ ) using the Euler matrix

$$\chi_{XYZ} = \sum_{xyz} U_{XYZ} \chi_{xyz} \quad (6)$$

The components of the transformation matrix depend on the Euler angles ( $\theta, \phi, \chi$ ), which relate the molecular and laboratory fixed coordinate systems. By integration over  $\phi$ , the twist angle, and  $\chi$ , the azimuthal angle, it is possible to plot the ratio of resonant intensities versus the tilt angle of the symmetry axis of the group being probed. A detailed description of the orientation calculation and the coordinate system used is detailed in an earlier publication.<sup>18</sup> This paper will be concerned with the stretching modes of the methyl group attached to the ring. The methyl group is assumed to have  $C_{3v}$  symmetry with free rotation along the  $C_3$  axis. From group theory we are able to determine which components of the hyperpolarizability tensor are allowed for each vibration. Therefore, methyl groups ( $C_{3v}$ ) are assumed to have  $\beta_{aac}$ ,  $\beta_{bbc}$ , and  $\beta_{ccc}$  as the hyperpolarizability tensor elements of symmetric stretching modes and  $\beta_{aca}$ ,  $\beta_{bcb}$ ,  $\beta_{caa}$ , and  $\beta_{cbb}$  as hyperpolarizability tensor elements of the antisymmetric modes. The other tensor elements ascribed to the antisymmetric vibrations integrate to zero when free rotation of the methyl group is assumed. This allows the components of the transformation matrix to be averaged over  $\phi$  and  $\chi$ , which, by comparing ratios of susceptibilities, leads to an equation that is only a function of the tilt angle  $\theta$ .

### Experimental Section

**Sum Frequency Generation Spectrometer.** The sum frequency generation spectrometer used is homemade; details of the setup have been described elsewhere.<sup>19</sup> The laser used to create the fundamental beam was a picosecond pulsed Nd:YAG (Ekspla) with a 20 Hz repetition rate. The fundamental (1064 nm) is used to pump an optical parametric generator/optical parametric amplifier OPG/OPA (Laservision) to create a frequency doubled fixed visible beam (532 nm) and an infrared beam tunable between 2000 and 4000  $\text{cm}^{-1}$ . The optical geometry adopted a copropagating configuration in which incidence angles of the visible and IR beams in air are 45° and 60°, respectively. Change of polarization of the incident laser beams was accomplished with the use of  $\lambda/2$  waveplates, and Glan-Laser polarizers were used to ensure the polarization combinations were correct for input and emitted beams. The SFG signal created at the surface was filtered from the 532 nm input beam and stray room light by optical filters and a monochromator, detected by a photomultiplier tube, and processed with a gated integrator. A computer program created in LabVIEW was used to collect the signal from the gated integrator and to scan the infrared frequency. The infrared frequency was scanned at 1  $\text{cm}^{-1}/\text{s}$ . Two polarization combinations, ssp (s-polarized SFG, s-polarized visible, and p-polarized

IR) and ppp, were acquired in the C–H stretching region from 2800 to 3100  $\text{cm}^{-1}$  for each sample. Each SFG spectrum was fitted in Origin 6.0 using a nonlinear curve fitting function (eq 3) with instrumental weighting for the error bars, which represents the standard deviation of the fit. Data presented here are an average of 10 scans of the infrared frequency over the desired range. The infrared beam reflected from the sample surface was collected with a Molelectron Energy Max 500 laser energy meter to correct for fluctuations in energy during the scan.

**Sample Preparation.** Disk electrodes (99.999+% pure) of 8 mm in diameter and 4 mm in thickness were used for all experiments. The electrodes were mounted in a Teflon holder and mechanically polished with sequential grits of diamond paste down to a 1  $\mu\text{m}$  finish and sonicated in ethanol between each step. The electrodes were then mechanically polished with 0.3 and 0.05  $\mu\text{m}$  alumina paste, with sonication in water between steps. This process produced a mirrorlike surface.<sup>20</sup> For copper electrodes, after the final sonication, the electrode was immediately placed in pure degassed phosphoric acid to protect the surface from contamination and oxidation until ready to use. The copper surface was then electropolished in a 50/50 solution of phosphoric acid and Millipore water (>18.2 M $\Omega$  cm resistivity and <5 ppb total organic carbon). The potential was swept from  $-500$  to  $1200$  mV at  $5000$  mV/s. This was done to remove the surface oxide layers and to adsorb a monolayer of phosphate, which kept oxide from forming. Millipore water was used to rinse the copper electrode repeatedly, and a droplet of water was left on the electrode surface to protect it during transfer to the electrochemical cell. Solutions were prepared using perchloric acid (Ultrex II, Baker), lead(II) perchlorate trihydrate (ACS grade, Aldrich), 5-methylBTAH (Aldrich), and ultrapure water (Millipore-Q). A 0.5 M perchloric acid solution was used as the electrolyte in all experiments.

For characterization of the copper electrodes, 5%  $10^{-4}$  M Pb(ClO<sub>4</sub>)<sub>2</sub> was added to the electrolyte. Underpotential deposition (UPD) coverage of lead was compared with ultrahigh vacuum (UHV) studies from the literature to ensure cleanliness and reproducibility.<sup>21,22</sup> By integration of the charge attributed to lead adsorption, the amount of lead on the metal surface was discerned. When the amount of lead adsorbed was compared with literature values, the fact that the same amount of metal sites were available for adsorption was confirmed. Platinum and gold electrodes were flame-annealed using the Clavilier method<sup>23,24</sup> and cooled in an argon gas atmosphere. The platinum and gold electrodes were checked for cleanliness by integrating the charge of the hydrogen UPD (platinum) and oxygen (gold) charge, respectively, to determine the coverage.

Cyclic voltammetry experiments were performed using a Pine bipotentiostat model AFBDP1 that was controlled by a computer. All cyclic voltammetry shown was performed at  $100$  mV/s scans using a saturated calomel electrode for the reference ( $0.24$  V vs normal hydrogen electrode). Electrochemical impedance spectroscopy measurements were performed using the M263A potentiostat in combination with a PAR M5210 lock-in amplifier controlled by PowerSINE software. The frequency range used was from  $100$  kHz to  $1$  Hz. The amplitude of the applied sinusoidal signal was  $5$  mV.

Sum frequency generation experiments were performed in a cell made of glass, Teflon, and Kel-F; a picture is shown in ref 25. This cell allows the potential of the working electrode to be controlled while SFG spectroscopy is performed. The thin layer of electrolyte allows the infrared beam to pass through the liquid layer with minimal adsorption. The thin layer

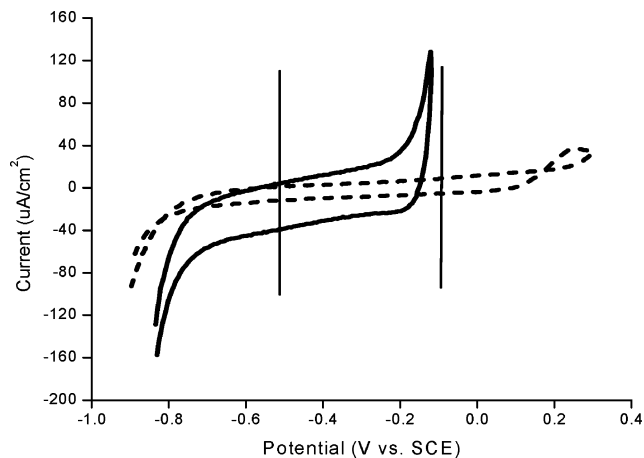


**Figure 2.** Cyclic voltammetry 0.5 M HClO<sub>4</sub> (solid line) and 50 mM 5-methylBTAH (dashed line) on polycrystalline copper. Vertical lines show the range of potential-dependent SFG.

electrochemical cell has an electrolyte layer that is  $5$ – $10$ - $\mu\text{m}$ -thick between the working electrode and the quartz window. The cell was cleaned by filling with a solution of  $50/50$  HNO<sub>3</sub>/H<sub>2</sub>SO<sub>4</sub> overnight and rinsing several times with Millipore water before use. The electrolyte solution,  $50$  mM 5-methylBTAH in  $0.5$  M HClO<sub>4</sub>, was purged with ultrahigh purity nitrogen for a minimum of  $30$  min before filling the cell. In situ cyclic voltammetry was used to ensure cleanliness and check electrical connections. The infrared beam reflected from the sample surface was collected to correct for fluctuations in energy during the scan. The infrared beam was attenuated by less than  $20\%$ , which was due to absorption from water.

To ensure that the SFG signal was from the electrode surface and not from the quartz window, spectra were collected with the electrode backed away from the quartz window. These spectra produced no SFG signal confirming that the interface being probed was the liquid/metal interface and not either the air/quartz or quartz/water interface.

## Results and Discussion

**Cyclic Voltammetry. Polycrystalline Copper.** Cyclic voltammograms (CVs) of polycrystalline copper shown in Figure 2 were recorded under a nitrogen atmosphere by using the hanging meniscus configuration. Figure 2 (solid line) shows the cyclic voltammogram for polycrystalline copper in  $0.5$  M HClO<sub>4</sub>. A featureless double-layer region was observed between  $-750$  and  $-150$  mV. The anodic current starting at around  $-150$  mV is due to dissolution of copper. The cathodic current starting at around  $-750$  mV is due to hydrogen evolution. When  $50$  mM of 5-methylBTAH was added (Figure 2, dashed line) the double-layer region increased by around  $450$  mV. The anodic current peak due to dissolution of copper did not occur until a potential of  $+300$  mV. This is believed to occur because the chemisorbed 5-methylBTAH blocks the surface, preventing copper dissolution.<sup>5</sup> The cathodic current seems less affected by the addition of 5-methylBTAH. The thickness of the double-layer region of the CV with  $50$  mM 5-methylBTAH added also decreases significantly.

**Polycrystalline Platinum.** Figure 3 shows the cyclic voltammograms for polycrystalline platinum in pure  $0.5$  M HClO<sub>4</sub> (solid line) and with  $50$  mM 5-methylBTAH added (dashed line). The cyclic voltammogram of polycrystalline platinum in pure electrolyte shows characteristic hydrogen adsorption from  $-250$  to  $0$  mV and an oxygenated species at  $450$  mV consistent with voltammograms of platinum in perchlorate solution.<sup>26–30</sup>

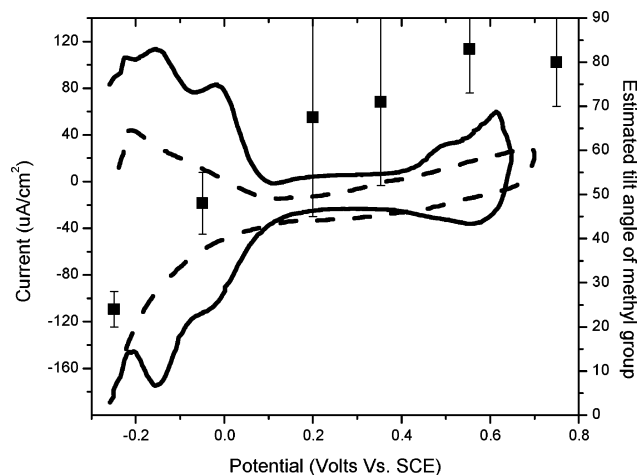


**Figure 3.** Cyclic voltammety 0.5 M HClO<sub>4</sub> (solid line) and 50 mM 5-methylBTAH (dashed line) on polycrystalline platinum (left axis) and orientation of 5-methylBTAH (squares) as a function of potential (right axis).

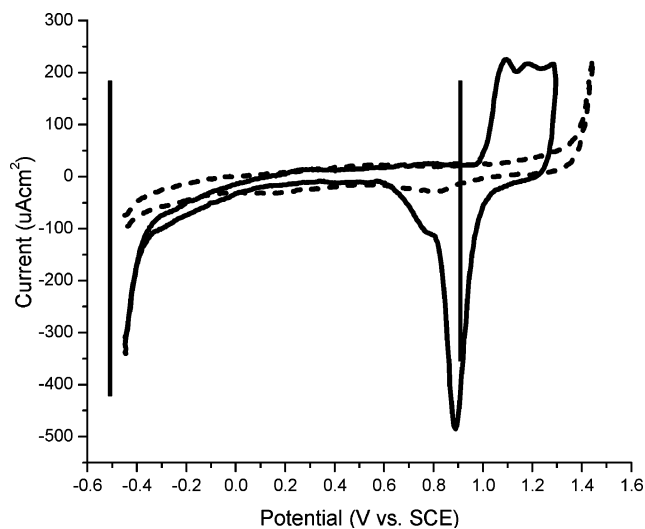


**Figure 4.** Cyclic voltammety 0.5 M HClO<sub>4</sub> (solid line) and 50 mM 5-methylBTAH (dashed line) on polycrystalline gold. Vertical lines show the range of potential-dependent SFG.

Addition of 5-methylBTAH causes a reduction of the amount of hydrogen absorbed to the surface and blocks the adsorption of oxygenated species to the surface. The blocking of the oxygenated species is evidence that 5-methylBTAH adsorbs to platinum surfaces.

**Polycrystalline Gold.** Figure 4 shows the cyclic voltammograms for polycrystalline gold in pure 0.5 M HClO<sub>4</sub> (solid line) and with 50 mM 5-methylBTAH added (dashed line). For the pure electrolyte voltammogram, the anodic current starting at 1000 mV is due to the absorption of oxygen species, and the cathodic peak at 900 mV is due to the reduction of oxygen from the surface.<sup>31</sup> When 50 mM 5-methylBTAH is added the oxygen absorption peak is shifted from a potential of 1000 to 1400 mV. The increase of the onset of oxygen absorption by 400 mV is believed to be due to the adsorption of 5-methylBTAH, which blocks the sites available for oxygen adsorption.

**Vibrational Assignments of 5-Methylbenzotriazole.** There have been no studies on the vibrational assignments in the C–H stretching region of 5-methylBTAH within the literature; therefore peak assignments were based on ab initio calculations and studies performed on benzotriazole<sup>11,32</sup> in determining C–H ring vibrations and toluene,<sup>33–35</sup> *p*-tosylate,<sup>36</sup> and 5-methylindole<sup>37</sup> for the methyl group.

**TABLE 1: 5-Methylbenzotriazole Vibrations**

SFG (cm <sup>-1</sup> )	assignment	ab initio (cm <sup>-1</sup> )
2880	Fermi resonance	
2920	symmetric methyl stretch	3187
2950	out-of-plane antisymmetric stretch	3243
2975	in-plane antisymmetric stretch	3275
	antisymmetric H–C(6)C(7)–H stretch	3356
	antisymmetric H–C(6)C(7)–H H–C(4) stretch	3389
3050	symmetric H–C(6)C(7)–H H–C(4) stretch	3393

Ab initio calculations were performed to determine the vibrational modes of 5-methylBTAH (Figure 1) using PC Spartan and Gaussian 98. These calculations were compared with vibrational assignments of similar molecules within the C–H stretching region, and the results are summarized in Table 1. Ab initio calculations are known to overestimate the calculated vibrational frequencies by around 10%,<sup>38</sup> but the relative ordering of the modes is usually reliable. The methyl group has been assigned the following vibrations: a symmetric methyl stretch at 2920 cm<sup>-1</sup>, an out-of-plane antisymmetric CH<sub>3</sub> mode at 2950 cm<sup>-1</sup>, and an in-plane CH<sub>3</sub> antisymmetric stretch at 2975 cm<sup>-1</sup>. This large splitting of the antisymmetric doublet is thought to be due to the C<sub>s</sub> symmetry of the molecule and to the fact that the methyl group is attached to an aromatic ring.<sup>36,37</sup> A Fermi resonance of the overtone of the asymmetric bending mode of the methyl group has been assigned at 2880 cm<sup>-1</sup>. The ring modes of the molecule have been calculated to be an antisymmetric H–C(3)C(4)–H mode at 3020 cm<sup>-1</sup> and a symmetric H–C(3)C(4)–H, H–C(6) mode at 3050 cm<sup>-1</sup>. The relative Raman intensity calculated using Gaussian predicts that the aromatic C–H vibrations should have less intensity than the methyl stretches.

**Sum Frequency Generation Spectroscopy. Polycrystalline Copper.** In situ SFG spectra of 5-methylBTAH adsorbed on polycrystalline copper are displayed in Figure 5. Two different polarization combinations are shown. The spectra on top were recorded with ppp (p-polarized sum frequency, p-polarized visible, and p-polarized infrared) polarization. The bottom spectra were recorded with an ssp input/output polarization combination. Spectra were taken at three different potentials, (A) –500, (B) –300, and (C) –100 mV, all within the double-layer region of the cyclic voltammogram (vertical lines in Figure 2). The potential-dependent spectra were confined to these potentials due to roughing of the electrode at potentials both positive and negative of this range because of the amount of time required to collect spectra (~1 h). Both ppp and ssp spectra are relatively constant for the potentials that were studied and are not dependent on the direction of the change in potential. Gewirth et al. did not observe a change in the SFG spectra of benzotriazole within the same potential region.<sup>10</sup> The ppp spectra show four resonances: the symmetric methyl stretch, the out-of-plane antisymmetric stretch, an in-plane antisymmetric stretch, and the symmetric ring mode from the benzene ring. The weakness of the C–H ring vibrations is attributed to the low Raman cross-section.<sup>11,32</sup> The ssp spectra show the same four vibrations, but the interference of the resonant and nonresonant contributions is not the same. An estimate of the orientation of 5-methylBTAH on polycrystalline copper is explained in a later section. To gain more information about how 5-methylBTAH adsorbs to metal electrodes, SFG spectra of 5-methylBTAH on polycrystalline platinum and polycrystalline gold were recorded.

**Polycrystalline Platinum.** Sum frequency generation spectra of 50 mM 5-methylBTAH on polycrystalline platinum were collected at six different potentials and two polarization

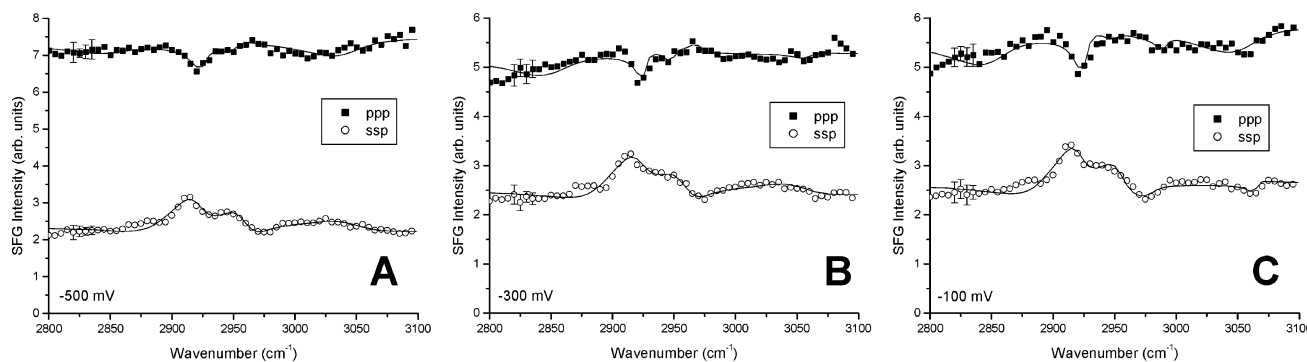


**Figure 5.** Potential-dependent SFG spectra of 50 mM 5-methylBTAH on polycrystalline copper with ppp polarization (top) and ssp polarization (bottom): (A)  $-500$  mV vs SCE, (B)  $-300$  mV vs SCE, (C)  $-100$  mV vs SCE.

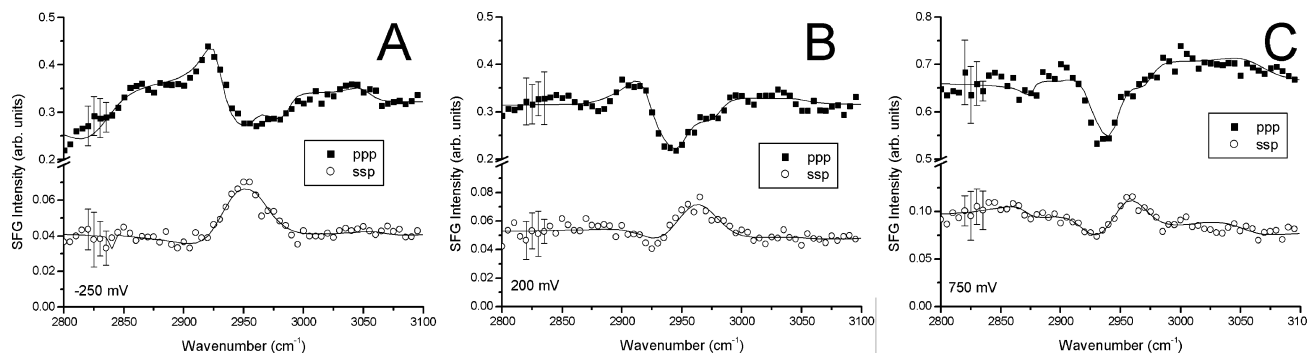


**Figure 6.** Potential-dependent SFG spectra of 50 mM 5-methylBTAH on polycrystalline platinum with ppp polarization (top) and ssp polarization (bottom): (A)  $-250$  mV vs SCE, (B)  $200$  mV vs SCE, (C)  $750$  mV vs SCE.

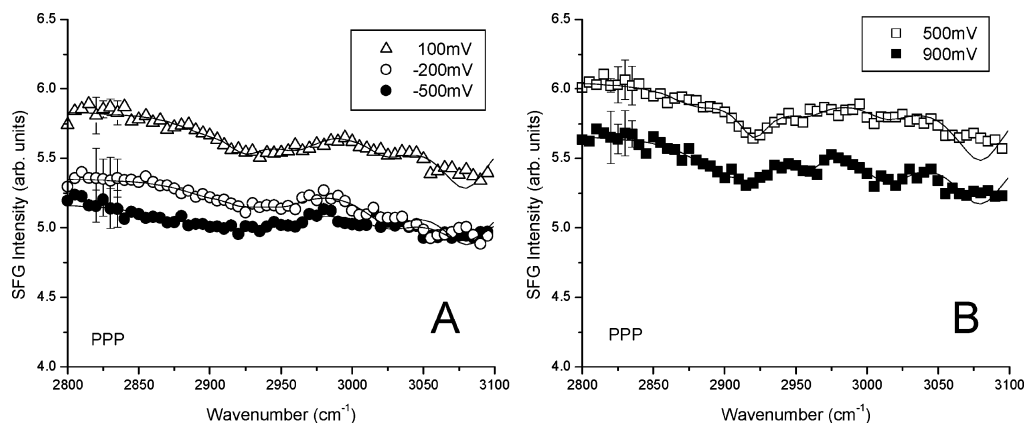


**Figure 7.** Potential-dependent SFG spectra of 50 mM 5-methylBTAH on polycrystalline gold with ppp polarization: (A)  $-500$ ,  $-200$ , and  $100$  mV vs SCE, (B)  $500$  and  $900$  mV vs SCE.

combinations. Sum frequency generation spectra of three of the potentials are shown in Figure 6. Unlike the copper system, the spectra of 5-methylBTAH on platinum show a change with potential. The change in spectra with potential is reversible and not dependent on the direction of change in potential. For the ppp (top) spectra, as the potential becomes more positive the amplitudes of the symmetric methyl peak at  $2920\text{ cm}^{-1}$  and the Fermi resonance at  $2880\text{ cm}^{-1}$  decrease, and the sizes of the antisymmetric methyl stretches increase. For the ssp (bottom) spectra, as the potential becomes more positive the amplitude of the symmetric methyl dip at  $2920\text{ cm}^{-1}$  increases, and the amplitudes of the antisymmetric methyl resonances also increase. The orientation of 5-methylBTAH on platinum at each potential studied was estimated and will be discussed in the following section.

**Polycrystalline Gold.** Sum frequency generation spectra of 50 mM 5-methylBTAH on polycrystalline gold collected with the ppp polarization combination at five different potentials are

shown in Figure 7. The ssp-polarized spectra were featureless and are not shown. The spectra on the left (A) were taken at  $-500$ ,  $-200$ , and  $100$  mV; these spectra are featureless, which suggests that 5-methylBTAH is not oriented on the surface or is oriented with the ring parallel to surface. At more positive potentials (B)  $500$  and  $900$  mV a resonance at  $2920\text{ cm}^{-1}$ , the  $\text{CH}_3$  symmetric stretch, appears. It is not feasible to perform an orientation calculation of 5-methylBTAH on gold due to the lack of resonances in the spectra at negative potentials, and the low signal-to-noise ratio of the spectra at more positive potentials also is prohibitive. Therefore only qualitative statements can be made to characterize the interface. By comparison of the cyclic voltammetry and the SFG spectra it is not possible to determine if 5-methylBTAH is adsorbed to the gold electrodes at negative potentials, but the molecule could be lying flat on the gold surface (the resonance must have a component of its transition dipole in the  $z$ -direction to be visible in ssp and ppp-polarized SFG spectra) or have a random orientation. There is

evidence in both the cyclic voltammetry and the SFG spectra that 5-methylBTAH is adsorbing at more positive potentials due to the resonance in the SFG spectra and the blocking of oxygen adsorption in the cyclic voltammogram (Figure 4). Since randomly oriented molecules do not produce SFG signals, this shows that the molecule has a polar orientation on the surface at positive potentials. These results suggest 5-methylBTAH adsorbs on polycrystalline gold with no preferential orientation or is lying parallel to the surface at negative potentials and begins to orient at more positive potentials. These results are similar to a study performed by Tadjeddine et al. using SFG to study 4-cyanopyridine on Au(111).<sup>39</sup> They observed that the pyridine ring was adsorbing parallel to the surface plane at intermediate potentials and began to orient more perpendicular to the surface at more positive potentials.

**Orientation Calculation.** Because the  $C_3$  axis of methyl group is in the same plane as the ring, by determination of the orientation of the methyl group it is possible to formulate a model for the orientation of the entire molecule. A detailed description of the orientation calculation for the methyl group of the polycrystalline copper/5-methylBTAH and polycrystalline platinum/5-methylBTAH is not possible because of several limiting factors. The methyl group's symmetry must be described using  $C_s$  symmetry, apparent from the splitting of the antisymmetric modes of the methyl group, instead of  $C_{3v}$  symmetry. The roughness of the metal surfaces also complicates the model used to determine orientation information. Determination of the hyperpolarizability tensor elements is critical to accurately calculate the orientation of adsorbed molecules with SFG spectroscopy. Difficulty in determination of the components of the infrared and Raman transition dipole moments remains a limiting step for orientation analysis.<sup>36,40</sup>

These limitations forbid detailed orientation calculations for the systems studied in this work. Orientation calculations were performed but will only be used to qualitatively describe the interfaces studied.

**Polycrystalline Copper.** For polycrystalline copper, comparison of the symmetric and antisymmetric methyl stretches produced an estimated tilt angle of  $\sim 45^\circ$ . Because the SFG spectra did not change with potential the orientation of 5-methylBTAH is not potential-dependent within the range studied. Since the  $pK_a$  of benzotriazole is 8.38,<sup>41</sup> the amine hydrogen is not expected to dissociate in such acidic solution. 5-Methylbenzotriazole is thought to be physically adsorbed to the surface, not chemically bonded. Leygraf and co-workers, using infrared reflection absorption spectroscopy, have reported that benzotriazole is oriented  $40^\circ$  from normal and expect 5-methylBTAH to have a more vertical orientation.<sup>9</sup> The similarities of the results from the two studies suggest that the orientation of benzotriazole on copper is not highly dependent on surface preparation since the study of Leygraf and co-workers was done ex situ, the electrolyte used for their study was NaCl, and copper oxide films were used as a substrate. Leygraf and co-workers have also performed potential-dependent in situ surface-enhanced Raman spectroscopy of benzotriazole on copper.<sup>12</sup> They also concluded that potential did not influence orientation.

**Polycrystalline Platinum.** Polycrystalline platinum spectra show a difference with potential. As the potential becomes more positive the amplitude of the methyl symmetric mode decreases, and the amplitudes of the methyl antisymmetric modes increase. The estimated tilt angle of the methyl group was plotted versus the applied potential and is shown in Figure 3. Figure 3 suggests that as the potential is increased the methyl group of 5-methylBTAH becomes more tilted from the surface normal. The

orientation angles plotted in Figure 3 are not implied to be a quantitative measurement of the orientation of 5-methylBTAH on platinum, only to show the qualitative trend.

The orientation of a similar molecule, pyridine, is known to be dependent on both coverage and temperature.<sup>42</sup> At low coverages pyridine is  $\pi$ -bonded oriented parallel to the surface plane; as the coverage is increased the molecule tilts toward the surface normal. Studies of several pyridine derivatives adsorbed on Pt(111) determined, by electron energy-loss spectroscopy (EELS), that a tilt angle between  $25^\circ$  and  $30^\circ$  from normal was the most common.<sup>43</sup>

Competitive coadsorption has been shown to cause reorientation of aromatic compounds adsorbed to platinum electrodes.<sup>44</sup> Studies of pyridine adsorption on platinum have shown that there is a competitive coadsorption of hydrogen (or oxygen) at a negative (or positive) potential range.<sup>45</sup> The absorption of hydrogen on the platinum electrode could be blocking sites for 5-methylBTAH adsorption thus affecting its orientation. By comparison of the cyclic voltammetry with the SFG spectra it is clear that there is hydrogen adsorbed at the most negative potentials studied. It is believed that the coadsorption of hydrogen has a large influence on the orientation of 5-methylBTAH adsorbed to platinum, as is the case with pyridine. The adsorbed hydrogen blocks sites for  $\pi$ -bonding of the benzene ring of 5-methylBTAH to the platinum surface. This causes the molecule to tilt more toward normal. As the hydrogen is removed the ring then changes orientation because the sites for  $\pi$ -bonding become available.

An interesting question that has arisen from this study is why 5-methylBTAH's orientation is potential-dependent on the platinum surface but not on the copper surface. This same effect has been seen for temperature-dependent studies of pyridine on Pt(111) and Cu(110).<sup>42</sup> This study used infrared spectroscopy to probe the two systems at different temperatures. On Cu(110), pyridine was orientated parallel to the surface and was not temperature-dependent. The orientation of pyridine on Pt(111) was temperature-dependent; at lower temperatures pyridine was oriented in the plane of the surface, and at 300 K pyridine was oriented with the surface normal. Comparison of these results with the findings of this paper suggests that the affinity of these types of molecules to adsorb to copper is stronger than to platinum.

The difference in orientation for the copper and platinum spectra may be due to several possibilities: hydrogen coadsorption on the platinum surface causing the 5-methylBTAH to tip up, the difference in the potential of zero charge (pzc) of the platinum and copper electrodes, or the ability of the triazole group to form a polymeric complex with copper ions in solution as well as the copper surface, which would bind the 5-methylBTAH more strongly to the surface.

Hydrogen coadsorption to the platinum electrode would block sites for adsorption of 5-methylBTAH. This effect could cause the orientation of 5-methylBTAH to be affected. Because of roughening of the copper surface at potentials outside the region studied, it was not feasible to probe potentials near hydrogen evolution to see if adsorbed hydrogen would cause a change in orientation for the copper system.

**Determination of the Potential of Zero Charge of Polycrystalline Copper.** Electrochemical impedance spectroscopy was performed to determine the difference in pzc between the copper and the platinum electrodes. Electrochemical impedance spectroscopy was performed on polycrystalline copper immersed in 0.5 M HClO<sub>4</sub> from  $-600$  to  $-100$  mV every 50 mV. Electrochemical impedance spectra were fit using a R(QR)

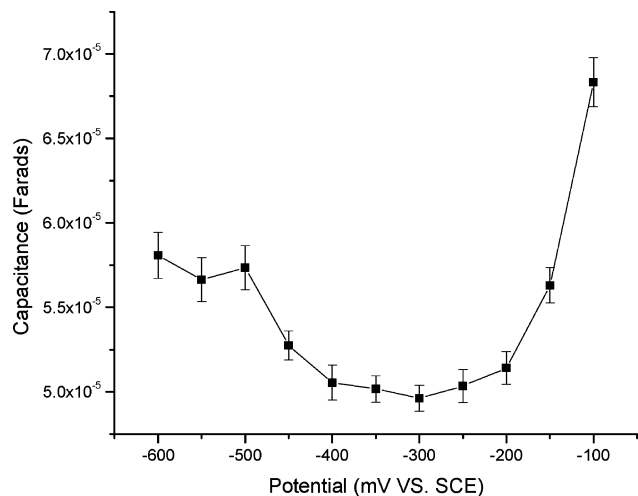


**Figure 8.** Capacitance vs potential plot of polycrystalline copper 0.5 M HClO<sub>4</sub>.

equivalent circuit, where R and Q represent a resistor and constant phase element, respectively. Parentheses denote that the two elements are in parallel. The constant phase element was used instead of a capacitor to obtain more accurate fits to the experimental data. The capacitance data were plotted versus potential to determine the pzc (Figure 8). The pzc was determined by finding the minimum capacitance of the curve. The pzc was determined to be approximately  $-300$  mV vs saturated calomel electrode (SCE). The pzc's of Cu(111) have been reported at values between  $-165$  and  $-472$  mV vs SCE.<sup>46,47</sup> From differential capacity measurements, the pzc of polycrystalline platinum in perchloric acid solution has been estimated to be about  $30$  mV vs SCE.<sup>30,48</sup> The difference of the pzc of the two metals is estimated to be around  $300$ – $400$  mV. If the charge on the electrode had a major role in the orientation of 5-methylBTAH, then the electrostatic attraction would be different on each side of the pzc causing a change in orientation. By comparison of the orientation of 5-methylBTAH on both sides of the pzc for both the copper and the platinum systems it is clear that charge does not play a large role in orientation. This leads to the assumption that the difference in the pzc of the two systems is not the cause of the change in orientation. Because the copper and platinum systems cannot be probed at the same potentials, it is unclear how much of an effect the potential has on the strength of the adsorption of 5-methylBTAH.

The most probable cause for why the orientation of 5-methylBTAH is not dependent on potential for copper but is for platinum is the ability of the triazole group to form a polymeric complex with copper ions in solution versus the weak adsorption of the triazole group on platinum. Benzotriazole forms an adsorbed adlayer at negative potentials and acidic pH, whereas the loss of the amine hydrogen at more positive potentials and basic pH causes a polymerized Cu(I)–BTAH complex to form.<sup>13</sup> It is unclear in these studies if 5-methylBTAH is coordinated only to the surface or if it is coordinated to the surface and copper ions. This effect has been seen in other surface studies of benzotriazole on copper.<sup>9,10</sup> The coordination of 5-methylBTAH to copper ions in addition to the surface could cause 5-methylBTAH to bind to the copper surface more strongly and therefore be insensitive to potential.

## Conclusions

Potential-dependent SFG spectroscopy was performed in situ to study the interfacial properties of 5-methylBTAH adsorbed

on polycrystalline copper, polycrystalline platinum, and polycrystalline gold. The CH<sub>3</sub> and aromatic C–H vibrations are used to identify adsorption and orientation of 5-methylBTAH at the three different metal electrode surfaces. For copper surfaces, orientation of the molecule on the surface is not affected by potential within the window studied ( $-500$  to  $-100$  mV vs SCE). The methyl group of 5-methylBTAH was estimated to be oriented  $\sim 45^\circ$  from normal. Spectra of 5-methylBTAH on platinum show a change in orientation over the potential range studied ( $-250$  to  $750$  mV vs SCE). The orientation of the methyl group tilts more toward the plane of the interface as the potential is scanned in the positive direction. This is thought to be due to hydrogen coadsorption on the platinum surface at negative potentials. Sum frequency generation spectra of 5-methylBTAH on gold are featureless at negative potentials, suggesting a flat orientation, but began to tilt toward normal at more positive potentials over the potential range studied ( $-500$  to  $900$  mV vs SCE).

**Acknowledgment.** The authors gratefully acknowledge financial support from the University of Houston, the Texas Advanced Technology Program, and Champion Technologies.

## References and Notes

- (1) Katritzky, A. R. *Comprehensive Heterocyclic Chemistry*; Pergamon Press: New York, 1984; Vol. 5.
- (2) Polewska, W.; Vogt, M. R.; Magnussen, O. M.; Behm, R. J. *J. Phys. Chem. B* **1999**, *103*, 10440.
- (3) Vogt, M. R.; Polewska, W.; Magnussen, O. M.; Behm, R. J. *J. Electrochem. Soc.* **1997**, *144*, L113.
- (4) Biggin, M. E.; Gewirth, A. A. *J. Electrochem. Soc.* **2001**, *148*, C339.
- (5) Sugimasa, M.; Wan, L.; Inukai, J.; Itaya, K. *J. Electrochem. Soc.* **2002**, *149*, E367.
- (6) Ito, M.; Takahashi, M. *Surf. Sci.* **1985**, *158*, 609.
- (7) Aramaki, K.; Kiuchi, T.; Sumiyoshi, T.; Nishihara, H. *Corros. Sci.* **1991**, *32*, 593.
- (8) Chan, H. Y.; Weaver, M. J. *Langmuir* **1999**, *15*, 3348.
- (9) Tornkvist, C.; Thierry, D.; Bergman, J.; Liedberg, B.; Leygraf, C. *J. Electrochem. Soc.* **1989**, *136*, 58.
- (10) Schultz, Z. D.; Biggin, M. E.; White, J. O.; Gewirth, A. A. *Anal. Chem.* **2004**, *76*, 604.
- (11) Rubim, J.; Gutz, I. G. R.; Sala, O.; Orville-Thomas, W. J. *J. Mol. Struct.* **1983**, *100*, 571.
- (12) Thierry, D.; Leygraf, C. *J. Electrochem. Soc.* **1985**, *132*, 1009.
- (13) Youda, R.; Nishihara, H.; Aramaki, K. *Electrochim. Acta* **1990**, *35*, 1011.
- (14) Williams, C. T.; Beattie, D. A. *Surf. Sci.* **2002**, *500*, 545.
- (15) Hunt, J. H.; Guyot-Sionnest, P.; Shen, Y. R. *Chem. Phys. Lett.* **1987**, *133*, 189.
- (16) Du, Q.; Superfine, R.; Freys, E.; Shen, Y. R. *Phys. Rev Lett.* **1993**, *70*, 2313.
- (17) Zhu, X. D.; Suhr, H.; Shen, Y. R. *Phys. Rev B* **1987**, *35*, 3047.
- (18) Zhang, H.; Romero, C.; Baldelli, S. *J. Phys. Chem. B* **2005**, *109*, 15520.
- (19) Baldelli, S. *J. Phys. Chem. B* **2003**, *107*, 6148.
- (20) Clavilier, J.; Armand, D.; Sun, S. G.; Petit, M. *J. Electroanal. Chem.* **1986**, *205*, 267.
- (21) Brisard, G. M.; Zenati, E.; Gasteiger, H.; Markovic, N.; Ross, P. N. *Langmuir* **1995**, *11*, 2221.
- (22) Brisard, G. M.; Zenati, E.; Gasteiger, H.; Markovic, N.; Ross, P. N. *Langmuir* **1997**, *13*, 2390.
- (23) Clavilier, J.; El Achi, K.; Petit, M.; Rodes, A.; Zamakhchari, M. A. *J. Electroanal. Chem.* **1990**, *295*, 333.
- (24) Clavilier, J.; El Achi, K.; Rodes, A. *J. Electroanal. Chem.* **1989**, *272*, 253.
- (25) Rivera-Rubero, S.; Baldelli, S. *J. Phys. Chem. B* **2004**, *108*, 15133.
- (26) Lazarescu, V.; Clavilier, J. *Electrochim. Acta* **1998**, *44*, 931.
- (27) Gomez, R.; Orts, J. M.; Alvarez-Ruiz, B.; Feliu, J. M. *J. Phys. Chem. B* **2004**, *108*, 228.
- (28) Albalat, R.; Clavilier, J. *J. Electroanal. Chem.* **1992**, *330*, 289.
- (29) Herrero, E.; Feliu, J. M.; Wieckowski, A.; Clavilier, J. *Surf. Sci.* **1995**, *325*, 131.
- (30) Iwasita, T.; Xia, X. *J. Electroanal. Chem.* **1996**, *411*, 95.
- (31) Hoare, J. *J. Electrochem. Soc.* **1984**, *131*, 1808.
- (32) Bigotto, A.; Pandey, A. N.; Zerbo, C. *Spectrosc. Lett.* **1996**, *29*, 511.

- (33) Varsanti, G. *Assignments for Vibrational Spectra of Seven Hundred Benzene Derivatives*; John Wiley & Sons: New York, 1974; Vol. 1.
- (34) Balfour, W. J.; Fried, Y. *Can. J. Phys.* **1994**, *72*, 1218.
- (35) Hommel, E. L.; Allen, H. C. *Analyst* **2003**, *128*, 750.
- (36) Bell, G. R.; Li, Z. X.; Bain, C. D. *J. Phys. Chem. B* **1998**, *102*, 9461.
- (37) Sanyal, N. K.; Tripathi, S. R. *Indian J. Phys., B* **1984**, *58*, 105.
- (38) Hehre, W. J.; Radom, L.; Schleyer, P. V.; Pople, J. *Ab Initio Molecular Orbital Theory*; Wiley: New York, 1986.
- (39) Pluchery, O.; Zheng, W. Q.; Marin, T.; Tadjeddine, A. *Phys. Status Solidi A* **1999**, *175*, 145.
- (40) Wang, H.-F.; Gan, W.; Lu, R.; Rao, Y.; Wu, B.-H. *Int. Rev. Phys. Chem.* **2005**, *24*, 191.
- (41) Dean, J. A. *Lange's Handbook of Chemistry*; McGraw-Hill: New York, 1992.
- (42) Haq, S.; King, D. A. *J. Phys. Chem.* **1996**, *100*, 16957.
- (43) Stern, D. A.; Frank, D. G.; Gui, J. Y.; Lu, F.; Salaita, G. N.; Zapien, D. C.; Hubbard, A. T. *J. Am. Chem. Soc.* **1989**, *111*, 877.
- (44) Soriaga, M. P.; White, J. H.; Song, D.; Hubbard, A. T. *J. Phys. Chem.* **1984**, *88*, 2284.
- (45) Cai, W.; She, C.; Ren, B.; Yao, J.; Tian, Z.; Tian, Z. *J. Chem. Soc., Faraday Trans.* **1998**, *94*, 3127.
- (46) Foresti, M. L.; Pezzatini, G.; Innocenti, M. *J. Electroanal. Chem.* **1997**, *434*, 191.
- (47) Lukomska, A.; Sobkowski, J. *J. Electroanal. Chem.* **2004**, *567*, 95.
- (48) Hamm, U. W.; Kramer, D.; Zhai, R. S.; Kolb, D. M. *J. Electroanal. Chem.* **1996**, *414*, 85.